

Chaotic Current Self-oscillations in Doped, Weakly Coupled Semiconductor Superlattices for True Random Number Generation



Yaohui Zhang, Yaara Aviad and Holger T. Grahn

Abstract A weakly coupled semiconductor superlattice (SL) represents an almost ideal one-dimensional nonlinear dynamical system, the nonlinearity of which is due to sequential resonant tunneling between adjacent quantum wells. A great richness of nonlinear transport behavior has been observed in weakly coupled SLs, including periodic as well as quasi-period current self-oscillations and even driven as well as undriven chaos. Recently, spontaneous chaotic and quasi-periodic self-oscillations have been observed in doped GaAs/(Al,Ga)As SLs with 45% Al at room temperature. Based on this type of SLs, an *all-electronic* true random number generator has been demonstrated at room temperature with achievable bit rates of up to 80 Gbit/s, about two orders of magnitude larger than typical bit rates for currently available all-electronic true random number generators. The synchronization of chaos using these SLs has been demonstrated as a useful building block for various tasks in secure communications. The realization of chaotic SLs without external feedback and the synchronization among differently structured SLs open up the possibility for advanced secure multi-user communication methods based on large networks of coupled SLs.

Keywords Semiconductor superlattice · Spontaneous chaos · True random number generator · Synchronization

Y. Zhang

Key Laboratory of Nanodevices and Applications, Suzhou Institute of Nano-Tech and Nano-Bionics, Chinese Academy of Sciences, Suzhou 215125, China
e-mail: yhzhang2006@sinano.ac.cn

Y. Aviad

Department of Applied Mathematics, Jerusalem College of Technology,
93721 Jerusalem, Israel
e-mail: aviaday@gmail.com

Y. Aviad

Department of Physics, Bar-Ilan University, 52900 Ramat-Gan, Israel

H. T. Grahn (✉)

Paul-Drude-Institut für Festkörperelektronik, Leibniz-Institut im
Forschungsverbund Berlin e. V., Hausvogteiplatz 5–7, 10117 Berlin, Germany
e-mail: htgrahn@pdi-berlin.de

© Springer International Publishing AG, part of Springer Nature 2018
L. L. Bonilla et al. (eds.), *Coupled Mathematical Models for Physical and Biological Nanoscale Systems and Their Applications*, Springer Proceedings in Mathematics & Statistics 232, https://doi.org/10.1007/978-3-319-76599-0_2

1 Introduction

Undriven chaotic current self-oscillations in semiconductor superlattices (SLs) were discovered in the mid 1990s in doped, weakly coupled GaAs/AlAs SLs at low temperatures [1]. Because of the indirect nature of the band gap in AlAs together with the rather low energy of the X valley, Γ - X transfer from the GaAs wells through the AlAs barriers can easily occur by thermal excitation at elevated temperatures. However, in 2012, Huang et al. [2] demonstrated that, by using the highest direct barrier of $\text{Al}_{0.45}\text{Ga}_{0.55}\text{As}$ in GaAs/(Al,Ga)As SLs, spontaneous chaotic current self-oscillations are observable at room temperature. The frequency spectrum of the chaotic current self-oscillations ranges from 0 to 4 GHz. The corresponding devices are of sub-millimeter size so that they can be easily integrated in existing devices.

This type of SL was subsequently used to demonstrate *all-electronic* true random number generators with bit rates up to 80 Gbit/s [3]. In comparison, the highest bit rates of currently available all-electronic true random number generators are typically below 1 Gbit/s [4] so that this type of true random number generator would result in an increase of the current bit rate by about two orders of magnitude. These devices do not require external feedback or conversion to an electronic signal prior to digitization. The method is robust and insensitive to external perturbations. At the same time, its fully electronic implementation suggests scalability and minimal postprocessing in comparison to existing optical implementations of true random number generators.

More recently, chaos synchronization has been demonstrated as a useful building block for various tasks in secure communications, including a source of all-electronic ultrafast true random number generators based on room temperature spontaneous chaotic oscillations in this type of SL [5]. The emergence of several types of chaos synchronization has been experimentally demonstrated, e.g. leader-laggard, face-to-face, and zero-lag synchronization in network patterns of coupled SLs consisting of unidirectional and mutual coupling as well as self-feedback coupling. Chaotic SL oscillators without external feedback and the synchronization among differently structured SLs open up the possibility for advanced secure multi-user communication methods based on large networks of coupled SLs.

2 Electric-Field Domain Formation and Chaos in Semiconductor Superlattices

In this section, we will briefly review the formation of static electric-field domains in doped, weakly coupled SLs and present spontaneous current self-oscillations due to the formation of dynamic domains. Spontaneous current self-oscillations can be driven with an incommensurate sinusoidal voltage for a fixed bias into a chaotic regime, i.e. transitions between synchronization and chaos are observed via pattern-forming bifurcations. However, it is also possible for doped, weakly coupled SLs to exhibit undriven chaos, i.e. spontaneous chaotic current self-oscillations. For a

detailed review of the work performed at temperatures well below room temperature, see Ref. [6].

2.1 Electric-Field Domains

Applying an electric field to a weakly coupled SL results in nonlinear transport along the SL axis due to resonant tunneling between different subbands of adjacent quantum wells. The resulting drift velocity-electric field characteristic becomes nonlinear with resonances at field strengths corresponding to the energetic separation of the involved subbands divided by the SL period d and the electron charge e . Between these resonances, the current density will exhibit regions of negative differential conductivity (NDC) and positive differential conductivity (PDC) as a function of the applied electric field. If carriers are added by for example doping the SL, the regions of negative differential conductivity become unstable, when the SL is biased in this region. For large carrier densities, static electric-field domains will form, where a region of a lower electric field F_{LFD} is separated by a charge accumulation layer (CAL), i.e. the domain boundary, from a region with a larger electric field F_{HFD} as shown in Fig. 1. LFD and HFD refer to the low-field and high-field domain, respectively. The values of F_{LFD} and F_{HFD} are in the PDC regions of the first and second resonance, respectively. The carrier density of the accumulation layer is determined by the difference of the electric field strengths of the two domains $F_{HFD} - F_{LFD}$ multiplied by the product of the relative permittivity ϵ of the material and the permittivity of the vacuum ϵ_0 divided by e .

2.2 Spontaneous Current Self-oscillations and Chaos

When the carrier density is reduced, the field distribution becomes unstable, resulting in spontaneous current self-oscillations, the frequency of which depends on the

Fig. 1 Schematic diagram of the distribution of the low- (F_{LFD}) and high-field domain (F_{HFD}) separated by a charge accumulation layer (CAL) in a doped, weakly coupled SL

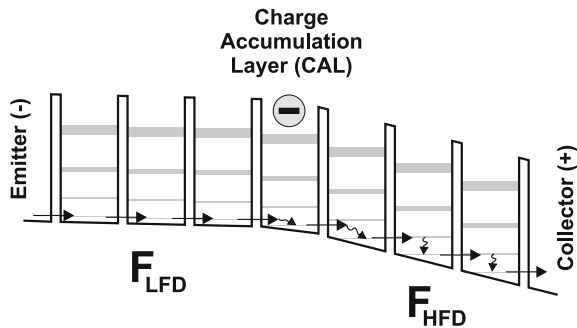
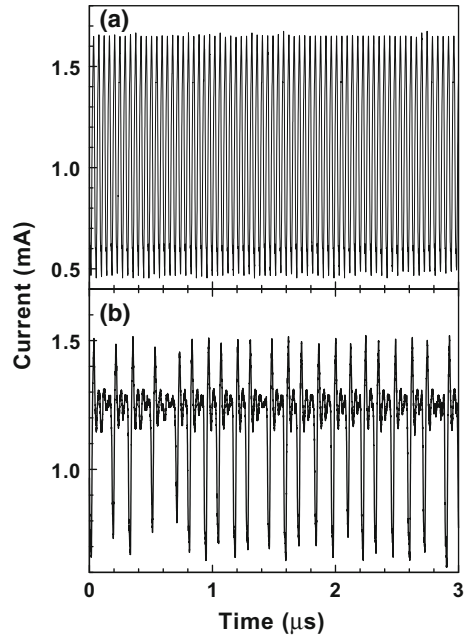


Fig. 2 Current oscillations in **a** the periodic regime at $V_{dc} = 7.6$ V and **b** the chaotic regime at $V_{dc} = 7.941$ V for the GaAs/AlAs SL recorded at 30 K [7]



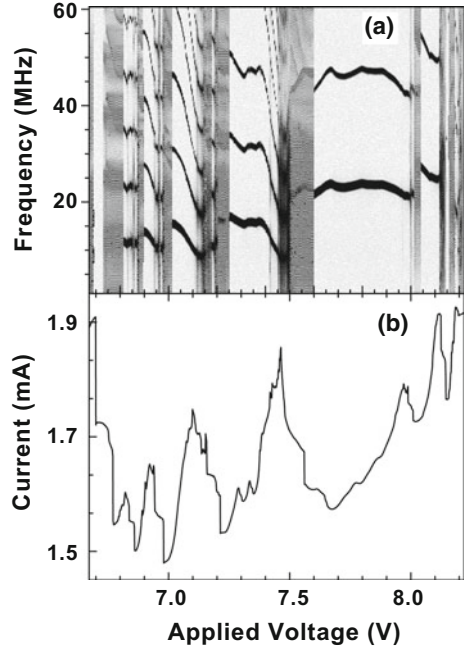
resonant coupling between adjacent wells. There are three types of current self-oscillations:

- spontaneous periodic,
- spontaneous quasi-periodic, and
- driven as well as spontaneous chaotic.

For spontaneous periodic current self-oscillations, either a charge monopole or a dipole, which represents the domain boundary, performs a recycling motion through the whole or part of the SL. For spontaneous quasi-periodic current self-oscillations, there is a competition between the dipole and monopole oscillation modes. Finally, chaotic current self-oscillations can be induced by driving the SL with an appropriate external voltage or can occur spontaneously.

Periodic current self-oscillations are shown in Fig. 2a for a GaAs/AlAs SL recorded for $V_{dc} = 7.6$ V at 30 K. The SL consists of 40 periods with 9.0-nm-thick GaAs wells and 4.0-nm-thick AlAs barriers. The central 5 nm of each GaAs well are doped with Si at $3 \times 10^{17} \text{ cm}^{-3}$. The corresponding frequency spectrum contains only two sharp peaks at 22 and 44 MHz. The time trace in Fig. 2a corresponds to a fully periodic regime with at least one higher harmonic. These oscillations occur in the second plateau of the time-averaged I - V characteristic in this sample. The time trace of the current becomes much more complex and irregular, when the applied voltage is changed to $V_{dc} = 7.941$ V as shown in Fig. 2b. The corresponding frequency spectrum consists of a broad-band noise spectrum. This time trace has the signature of undriven chaos.

Fig. 3 **a** Frequency spectra of the spontaneous current oscillations and **b** time-averaged current versus applied voltage for the GaAs/AlAs SL recorded at 30 K. In the power spectra, dark areas correspond to large amplitudes [7]



The existence of chaotic windows in the frequency spectra as a function of applied voltage becomes more evident when the power spectra for the GaAs/AlAs SL recorded at 30 K are plotted versus the applied voltage on a grey scale as in Fig. 3a. Dark areas correspond to a large amplitude of the oscillations. The corresponding time-averaged I - V characteristic is shown in Fig. 3b on the same voltage scale at the same temperature [1, 7]. With increasing bias, several chaotic windows exist, which are separated by periodic windows containing only the fundamental frequency and several higher harmonics. The transition from the chaotic to the periodic window occurs over a very narrow voltage range, e.g. at $V_{dc} = 7.6$ V. However, the transition from a periodic to a chaotic window usually consists of a random-enhancing process covering a broader voltage range. Comparing the voltage ranges of the chaotic windows with the time-averaged I - V characteristic in Fig. 3b, there is a clear correlation between the existence of a chaotic window and a large NDC in the time-averaged current. In contrast, the periodic windows appear for PDC.

The sharp transitions from the chaotic to the periodic window correspond to the minimum value of the average current, i.e. the onset of PDC. The regions with a PDC are characterized by attractive coupling between the different quantum wells. The SL behaves as a self-synchronized unit with spontaneous periodic current oscillations. However, in the regions with a large NDC, the coupling becomes strongly repulsive. With increasing repulsion, the synchronized oscillations become more and more destabilized, until the SL enters a chaotic state. With increasing temperature, the chaotic windows become smaller and smaller, until they completely disappear at 60 K

[7]. As the temperature increases, the thermal energies increase so that thermionic emission into the X valley of the AlAs barriers becomes more easily possible, since the energy separation between the Γ valley in GaAs and the X valley in AlAs is about 160 meV, while the difference between the Γ valleys of both materials is about 980 meV. In addition, other scattering mechanisms such as optical phonon scattering become more and more likely, thereby reducing the effective non-linearity of the system. The structures in the time-averaged I - V characteristic disappear completely for temperatures above 60 K in GaAs/AlAs SLs so that a structureless current plateau is a signature of a large periodic window. The undriven chaos itself is probably generated by the presence of the finite time scale of the sequential resonant tunnelling process between adjacent wells.

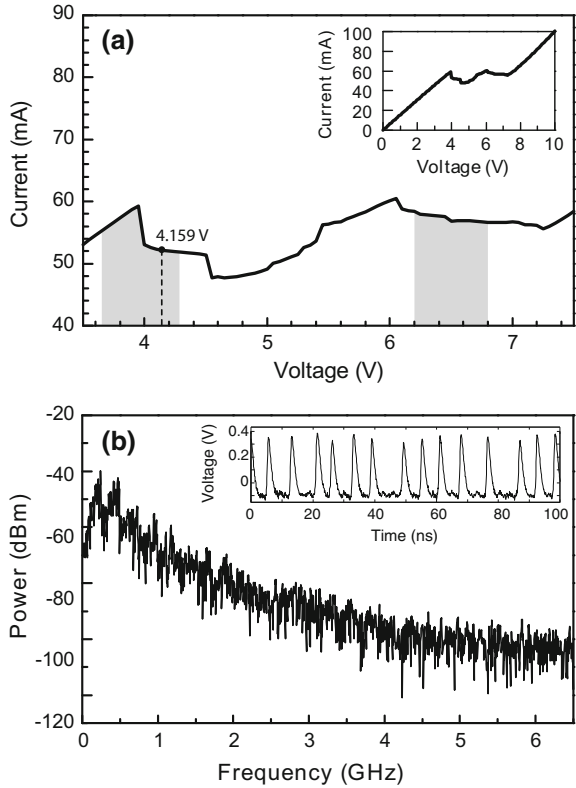
2.3 Spontaneous Current Self-oscillations at Room Temperature

In order to achieve spontaneous current self-oscillations in a weakly coupled SL at room temperature, the choice of the barrier material is crucial. To achieve the highest direct barrier in a GaAs/Al $_x$ Ga $_{1-x}$ As SL, the Al content x should be chosen with a value of about 0.45. In this case, the Γ and X valleys of the Al $_{0.45}$ Ga $_{0.55}$ As barrier are separated by about 390 meV from the Γ valley of GaAs so that the thermal excitation of electrons in the GaAs quantum wells over the (Al, Ga)As barrier can be effectively reduced. This suppression may provide the existence of the nonlinearity in SLs up to higher temperature so that spontaneous current self-oscillations can occur in GaAs/Al $_{0.45}$ Ga $_{0.55}$ As SLs even at room temperature. Indeed, spontaneous chaotic current self-oscillations have been observed experimentally in a GaAs/Al $_{0.45}$ Ga $_{0.55}$ As SL at 300 K in 2012 [2]. The SL consists of 50 periods with 7.0-nm-thick GaAs wells and 4.0-nm-thick Al $_{0.45}$ Ga $_{0.55}$ As barriers. The central 3.0 nm of each GaAs well are doped with Si at $3 \times 10^{17} \text{ cm}^{-3}$.

When this GaAs/Al $_{0.45}$ Ga $_{0.55}$ As SL is biased in the voltage range between 6.21 and 6.80 V, spontaneous chaotic current self-oscillations are observed. The corresponding frequency spectrum is very wide and very noisy with a frequency distribution ranging up to 4 GHz, providing a clear signature of spontaneous chaos [2].

Figure 4a shows the I - V characteristic of a GaAs/Al $_{0.45}$ Ga $_{0.55}$ As SL with similar parameters as in Ref. [2], but a different doping density of $2 \times 10^{17} \text{ cm}^{-3}$ in the GaAs well, recorded at 300 K. When the dc bias voltage ranges between 4 and 4.3 V as well as 6.2 and 6.8 V marked by the gray-shaded regions in Fig. 4a, the SL exhibits spontaneous chaotic current self-oscillations. The oscillation amplitude exceeds 0.4 V into a 50 Ω load resistor, corresponding to 8 mA, and the bandwidth amounts to several hundreds of MHz as shown in Fig. 4b. The frequency spectrum of these spontaneous chaotic current self-oscillations is so wide that it can be used as wideband noise source. The inset of Fig. 4b displays a 100-ns-long time trace, which was digitized at 40 GHz.

Fig. 4 a Plateau region of the I - V characteristic of the GaAs/Al_{0.45}Ga_{0.55}As SL consisting of two voltage segments (gray regions) characterized by chaotic current oscillations. Most of the measurements discussed in Sect. 3 were carried out at 4.159 V (dashed vertical line). The inset shows the I - V characteristic over the entire voltage range. **b** Spectrum of the chaotic oscillations [2]. Inset: a 100-ns-long time trace of the SL current oscillations [3]



Bonilla et al. [8] have discussed a mathematical model to describe spontaneous chaos in idealized SLs with identical wells and barriers. Their numerical simulations show that spontaneous chaos may possibly appear directly from a two-frequency quasi-periodic attractor. In addition, they demonstrated that the unavoidable shot and thermal noise, which exist in the SL, both enhance existing deterministic chaos and induce chaos in nearby voltage intervals. They also discussed that the differences between numerical and experimental results may be due to imperfections in the doping density, the Ga content in the barriers, and the size thereof. A better model has to be developed in order to discuss the imperfections and their effect on the chaotic oscillations.

Spontaneous quasi-periodic current self-oscillations have also been observed at room temperature in this GaAs/Al_{0.45}Ga_{0.55}As SL [9]. The underlying physical mechanism may be related to the interaction of two oscillation modes, namely, the collective dipole motion mode through the whole SL and the well-to-well hopping mode within a few SL periods. Furthermore, noise-enhanced chaos in a GaAs/Al_{0.45}Ga_{0.55}As SL has been observed at room temperature in experiments [10] as well as in the results of the simulation of nonlinear transport based on a discrete tunneling model [10, 11]. The investigated sample has nominally the same parame-

ters as in Ref. [3], but it was grown in a different place and a different time. When external noise is added, both the measured and simulated current-versus-time traces contain irregularly spaced spikes for particular applied voltages, which separate a regime of periodic current oscillations from a region of no current oscillations at all. Increased noise can consequently enhance chaotic current oscillations in SLs.

Finally, the presence of a coherence resonance has been experimentally identified in a doped, weakly coupled GaAs/AlAs SL at 77 K, which exhibits current self-oscillations when driven by noise [12]. The SL consists of 28 periods with 9.0-nm-thick GaAs wells and 4.0-nm-thick AlAs barriers. The central 5.0 nm of each GaAs well are doped with Si at $3 \times 10^{17} \text{ cm}^{-3}$. The physical mechanism is related to the interaction between the noise source and two oscillation modes of the SL oscillator: the well-to-well hopping mode and the dipole-motion mode. For a range of intermediate noise levels, the intrinsic oscillation mode of the SL oscillator, i.e. the well-to-well hopping mode, is activated, and the dipole motion is forced into a collective periodic oscillating state, resulting in a coherence resonance.

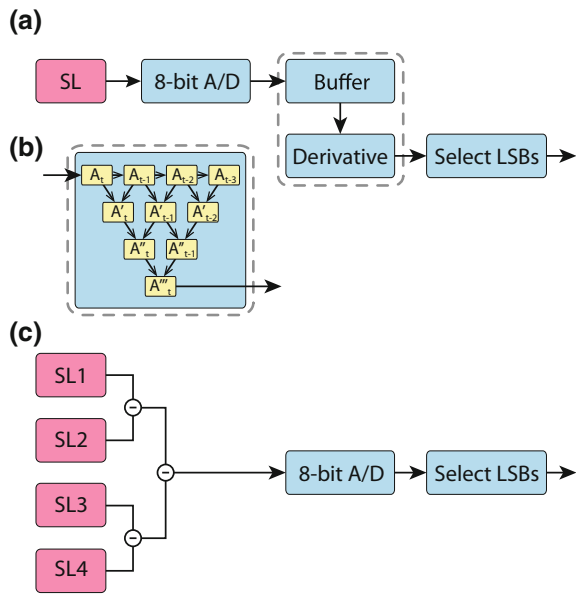
3 True Random Number Generator Based on GaAs/A_{0.45}Ga_{0.55}As Superlattices

In a true random number generator (TRNG), random numbers are produced from a stochastic physical process rather than a deterministic computer program. Currently, the bit rate of *all-electronic* TRNGs is typically below 1 Gbit/s [4]. These devices are often based on microscopic phenomena that generate low-level, statistically random noise signals such as thermal noise, the photoelectric effect, or quantum phenomena. In contrast, nonlinear electrical transport in SLs generates spontaneous chaotic current self-oscillations with GHz frequencies at room temperature, which may be used for TRNG devices. It is very important to increase the current bit rate of *all-electronic* TRNGs by several orders of magnitude for applications such as encryption, secure communication, stochastic computational codes, and electronic commerce.

Two methods have been used to generate a random bit sequence from the spontaneous chaotic current self-oscillations in GaAs/A_{0.45}Ga_{0.55}As SLs schematically shown in Fig. 5. The first method is similar to the already demonstrated *optical* TRNG scheme, where the generation of the random bit sequence consists of the following two steps [13]. In the first step, a dynamical buffer of the last $n + 1$ successively digitized electrical current values of the SL is used to calculate the n th discrete derivative as exemplified for $n = 3$ in Fig. 5b. In the second step, the m least significant bits (LSBs) of the resulting n th derivative are appended to the random bit sequence as shown in Fig. 5a. The second method consists of a linear combination of the analog chaotic current oscillations of several uncorrelated SLs as shown in Fig. 5c.

The time trace of the spontaneous chaotic current self-oscillations shown in Fig. 6a was digitized at 40 and 1.25 GHz as indicated by the blue line and red dots, respectively. Figure 6b shows the 1st and the 4th derivatives of the signal presented in Fig. 6a sampled at 1.25 GHz. Whereas for the first derivative [red line in Fig. 6b]

Fig. 5 **a** Schematic diagram of the TRNG method based on discrete time derivatives of the digitized current signal and retention of only a number of least significant bits (LSBs). **b** An example of the 3rd discrete derivative implementation of the method described in (a), where A_t stands for the digitized signal. **c** Schematic diagram of the parallel combination TRNG method where a minus sign stands for the subtraction, i.e., signal of SL1 minus the signal of SL2 [3]



there are many time points with near zero value, the fourth derivative values [blue line in Fig. 6b] fluctuate on all time scales. Retaining only the LSBs is still required to guarantee the generation of random sequences with verified randomness using the National Institute of Standards and Technology (NIST) statistical test suite [14]. Higher sampling rates than the 1.25 GHz used here, with the retention of 5 LSBs, require a much higher-order derivative; for example, a sampling rate of 5 GHz requires the 10th discrete derivative so as to pass the NIST statistical test. The implementation of higher derivatives requires a longer buffer and does not result in much improved bit rate generation. Using the first method, a bit rate of 6.25 Gbit/s was achieved using a sampling rate of 1.25 GHz, the 4th derivative, and a retention of 5 LSBs out of 8 bits.

The second method for implementing an SL-based TRNG overcomes these difficulties. Since the spike timings of independent SL devices are uncorrelated, one can linearly combine several such signals and “fill” the interspike intervals as shown in Fig. 6c for a linear combination of four recorded SL time traces digitized at 40 GHz. Because of the unavailability of several such SL devices in our experiment, this TRNG method was tested by combining segments with a large separation in time of the recorded current oscillations of a single device. The chaotic nature of the device ensures absence of any correlation between these segments. This method, as illustrated in Fig. 5c, requires only a single analog-to-digital converter regardless of the number of combined SL devices. To minimize the possible emergence of bias in the combined analog signals, each pair of signals is combined by subtraction. For example in Fig. 5c, the combined signal consists of $SL1 + SL4 - SL2 - SL3$. A 40 Gbit/s TRNG with verified randomness was obtained using a linear combination

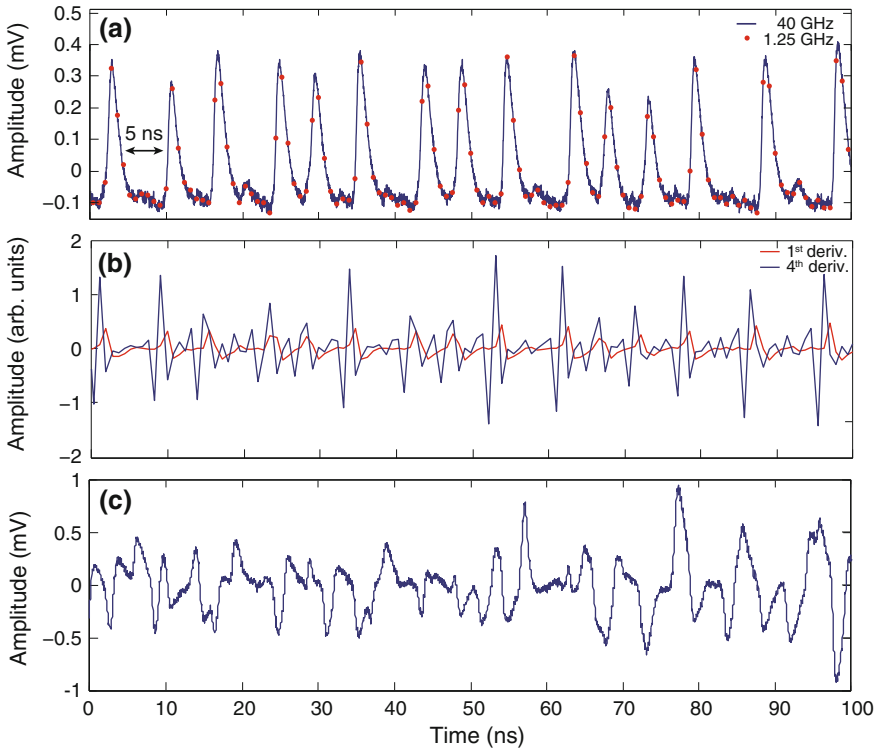


Fig. 6 **a** A 100 ns time trace of SL oscillations digitized at 40 (blue line) and 1.25 GHz (red dots). **b** 1st and 4th order discrete derivatives of the SL oscillations sampled at 1.25 GHz presented in panel (a). **c** Linear combination of four recorded SL time traces digitized at 40 GHz [3]

of four signals, a sampling rate of 10 GHz, and 4 LSBs. At a sampling rate of 20 GHz, the statistical NIST tests for randomness of this combination failed. However, a combination of six signals passed the statistical tests, resulting in a TRNG with a bit rate of 80 Gbit/s with verified randomness. This value is about two orders of magnitude larger than the bit rates for currently available *all-electronic* TRNGs. Because of the submillimeter dimensions and all-electronic nature of the SL devices, they can be easily integrated into existing devices.

Table 1 summarizes several key points of the tested parameter space according to the order of the derivative and the number of combined independent SL signals for the retention of 5 or 4 LSBs. For a single SL sampled at 1.25 GHz and 5 LSBs retained, at least the 4th order derivative is required to generate a verified random sequence resulting in a bit rate of 6.25 Gbit/s for the TRNG. When the sampling rate is increased to 5 GHz, higher derivatives become necessary even for fewer than 5 LSBs. Alternatively, a combination of both methods may be used at 5 GHz sampling rate with two SLs, a 3rd order derivative, and retention of 4 LSBs for a bit rate of 20 Gbit/s. The previously mentioned parallel combination of 4 and 6 SL devices with

Table 1 For a given number of combined independent signals, the TRNG bit rate is fixed by the sampling rate and the number of retained LSBs. The minimum order of derivative necessary for verified randomness is minimized to zero for four or more combined signals.

Number of combined SL devices	1	2	4	6
Derivative	4	3
Maximum sampling rate (GHz)	1.25	5	10	20
Retained LSBs	5	4	4	4
TRNG bit rate (Gbit/s)	6.25	20	40	80

a retention of 4 LSBs allows for a further increase of the sampling rate, resulting in bit rates of 40 and 80 Gbit/s, respectively, for the TRNG without the use of derivatives. The results demonstrate the interplay between the sampling rate, order of derivative, and number of combined SL signals. For a given number of retained LSBs, the rate of the TRNG can be enhanced either by increasing the number of combined SL signals or by increasing the order of the derivative.

4 Chaos Synchronization in Networks of GaAs/A_{0.45}Ga_{0.55}As Superlattices

The emergent synchronization of chaotic systems is a fundamental phenomenon in nonlinear dynamics with interesting applications for private- and public-channel secure-communication protocols, since messages can be concealed and transmitted by the synchronized chaotic signal. A variety of types of synchronization have been already observed between coupled chaotic oscillators including leader-laggard synchronization using unidirectional coupling and face-to-face synchronization using mutual coupling. In addition, zero-lag synchronization (ZLS) has been observed based on mutual coupling with an additional delayed self-feedback to each one of the chaotic lasers or by using multiple mutual couplings. In ZLS, chaotic oscillations are simultaneously synchronized in spite of an arbitrarily large physical distance between the chaotic oscillators. ZLS between two or more chaotic semiconductor lasers is of great current interest because of promising applications to public-channel cryptography without relying on the number theory, as in other existing methods.

The investigated SL devices have been obtained from the same wafer as the ones in Ref. [10]. We will first discuss the leader-laggard configuration. A chaotic SL A drives unidirectionally a nonchaotic SL B having a similar structure, applying no or a moderate bias voltage. The distance between the two SLs was set to 16 μm as indicated in Fig. 7a. The unidirectionality is attained by inserting a broadband amplifier into the connecting link that enhances the signal traveling from SL A to SL B, but not vice versa. Although the two SLs might differ somewhat in their I - V characteristics as well as in their chaotic voltage regions, their waveforms become highly synchronized with a delay of about 65 ns as shown in Fig. 7b. This delay originates

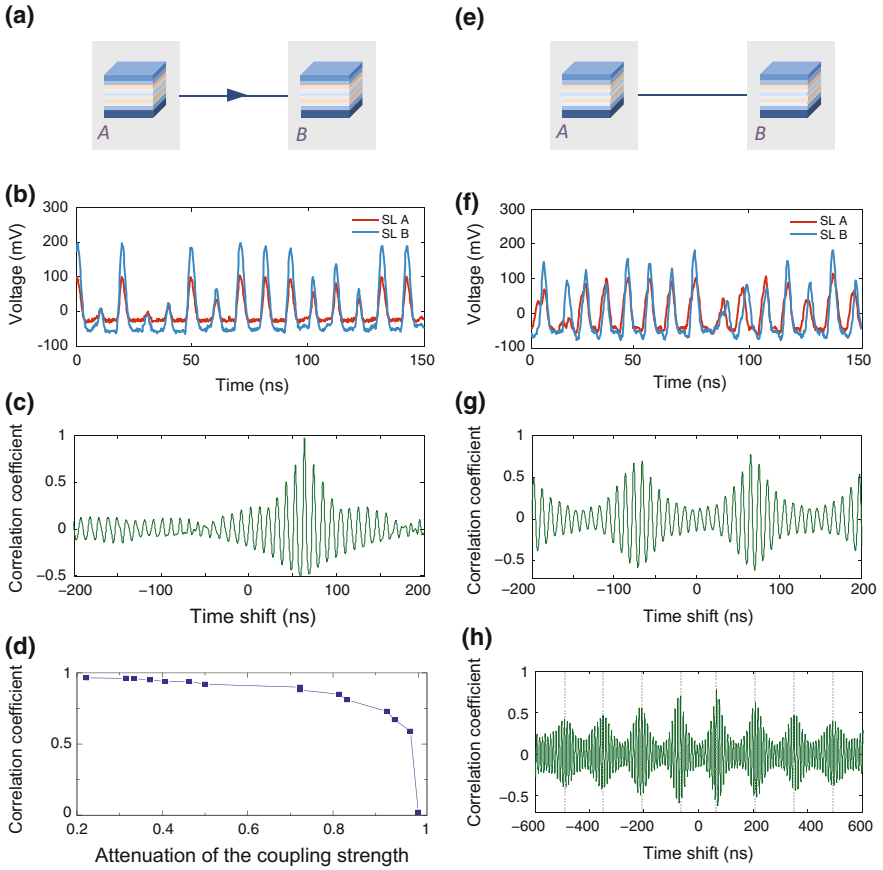


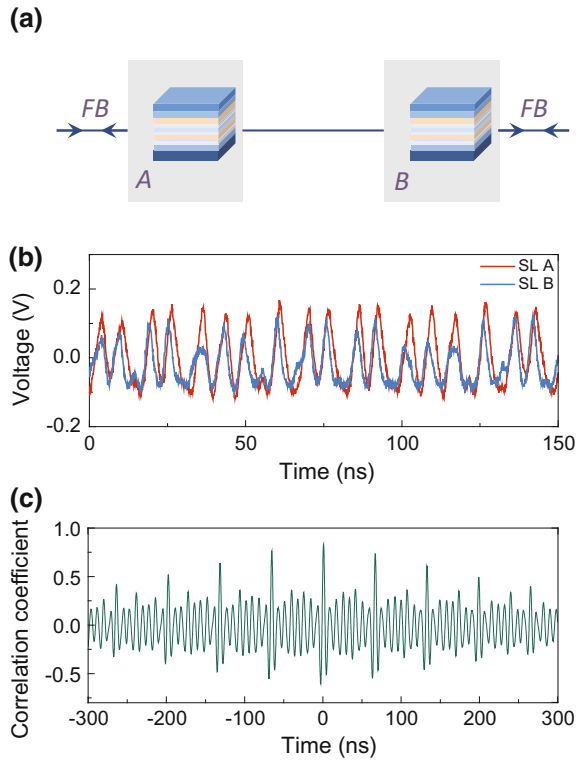
Fig. 7 **a** Schematic diagram of a leader-laggard setup with unidirectional coupling, which is realized by a broadband amplifier enhancing signals from SL A and transmitting them to SL B. **b** A snapshot of a 150-ns-long time trace of spontaneous chaotic current self-oscillations digitized at 5 GHz for SL A (blue) and SL B (red) shifted by 65 ns. **c** The cross-correlation between the current waveforms of the two SLs in **(a)**, indicating a nearly-unity correlation peak at about 65 ns, where any additional delay due to the amplifier is negligible. **d** Correlation coefficient of the leader-laggard synchronization as a function of attenuation of the coupling strength. **e** Schematic representation of a face-to-face setup similar to **(a)**, but without an amplifier. **f** Similar to **(b)** with the same shift to SL B. **g** The cross-correlation between the current waveforms of the two SLs indicating fairly good symmetry around zero delay and peaks at ± 65 ns. **h** Magnification of the cross-correlation in **(g)** indicating additional fading revival peaks at $\pm(2n + 1) \times 65$ ns (vertical dashed lines) with n being an integer [5]

from the 16-m-long unidirectional coupling corresponding to the velocity of the signal-propagating electric device. Quantitatively, the almost perfect leader-laggard synchronization, both in spike timings and in relative amplitudes of the spikes, is marked by a cross-correlation peak approaching one, which rapidly vanishes on a shifted time scale of several inter-spike-intervals as shown in Fig. 7c. Interestingly, the quality of the leader-laggard synchronization is found to be nearly insensitive to the coupling strength, which was measured by the height of the peaks in their correlation as a function of the coupling strength. The results indicate a high degree of synchronization even for relatively weak coupling as indicated in Fig. 7d. Moreover, unlike synchronization among coupled lasers which requires temperature control, the synchronization of coupled SLs is insensitive to the variation at room temperature.

Changing the unidirectional coupling to bidirectional by removing the amplifier results in a face-to-face configuration as shown in Fig. 7e. A snapshot of a 150-ns-long time trace of spontaneous chaotic current self-oscillations digitized at 5 GHz is shown in Fig. 7f for the face-to-face configuration. The symmetry between the two similarly structured SLs is now partially restored, where both SLs are now simultaneously leaders and laggards as well. To completely restore the symmetry, the voltage of the second SL B is enhanced in such a way that each isolated SL without the mutual connection is chaotic. This complete symmetry is now reflected in the symmetric cross-correlation function around the origin shown in Fig. 7g. Specifically, there are two similar dominant peaks around ± 65 ns related to the delay of the electric signal propagation between the two SLs. Since the output current of a SL typically increases with the applied voltage across the device (cf. Fig. 4a), one expects a quasi-periodic structure for the output current waveform due to the mutual coupling, which is also reflected by the cross-correlation function (cf. Fig. 7g). Indeed, the cross-correlation function exhibits fading revivals at about $(2n + 1) \times 65$ ns, where n is an integer as can be seen in Fig. 7g, h. Such revivals are absent in the leader-laggard setup (cf. Fig. 7c). Note that ZLS is another possible solution maintaining the symmetry between the two SLs. However, our experimental results indicate that ZLS becomes unstable in a face-to-face configuration.

The ability to achieve ZLS between two SLs, but without a relay mechanism, requires additional self-couplings as indicated in Fig. 8a. Here, the two SL devices, which both consist of 60- μ m-square mesas, are mutually connected with a 16-m-long cable between the top contact of SL A and the bottom contact of SL B. In addition, an 8-m-long cable was connected to the bottom contact of SL A, while its other terminal was open-circuited, and similarly an 8-m-long cable was connected to the bottom contact of SL B. Each of these two cables reflects from its open end a fraction of the chaotic signal back into its SL, hence functioning as a 16-m-long self-feedback connection. Consequently, the face-to-face solution shown in Fig. 7e is now an inconsistent solution, and the stable solution becomes ZLS with a dominant cross-correlation peak of about 0.84 at zero time shift as shown in Fig. 8b. The quasi-periodicity of the waveform is represented by fading revivals at about $n \times 65$ ns, where n is an integer, as opposed to about 2×65 ns time lags between revival peaks in the case of the face-to-face configuration (cf. Fig. 7h).

Fig. 8 **a** Schematic diagram of two mutually coupled SLs with a 16 m cable with an additional self-feedback (FB) coupling of 8 m for each SL. **b** A snapshot of a 150-ns-long time trace of spontaneous chaotic current self-oscillations of the SLs A (red) and B (blue). **c** Cross-correlation between the two SLs with a dominant ZLS peak of about 0.84 and fading revival peaks at about $n \times 65$ ns, where n is an integer [5]



Leader-laggard, face-to-face, and zero-lag types of synchronization were experimentally demonstrated among mutually coupled chaotic SLs at room temperature. In addition, the synchronization of different mesa shapes and sizes has been demonstrated in a star configuration using five SL devices [5]. Each type of synchronization clearly reflects the symmetry of the topology of its network pattern. The emergence of a chaotic SL without external feedback as well as the effective interaction between coupled, but differently structured SLs are distinguishing features of SLs as opposed to typical chaotic lasers. These features are expected to lead to the ability of synchronization of much larger scale patterns and hint on reliable as well as advanced secure communication protocols based on chaos synchronization.

5 Summary and Conclusions

Spontaneous chaotic current self-oscillations with a bandwidth of several GHz have been experimentally demonstrated in doped, weakly coupled GaAs/Al_{0.45}Ga_{0.55}As SLs at room temperature. The use of an (Al,Ga)As barrier with 45% Al content

instead of an AlAs barrier strongly reduces leakage currents induced by thermally excited Γ - X intervalley transfer. At the same time, the nonlinearity of these SLs is sufficiently strong to stimulate spontaneous chaos up to room temperature.

A high-speed, *all-electronic* true random number generator based on spontaneous chaotic current self-oscillations of GaAs/Al_{0.45}Ga_{0.55}As SL devices has been demonstrated experimentally operating at room temperature. The randomness of the generated sequences has been verified using a statistical test suite. The all-electronic method uses the parallel combination of multiple, independent SL signals, a single SL with high-order derivatives, or a combination of both methods, demonstrating a large degree of scalability and customization options, depending on TRNG rate requirements and complexity restrictions of the setup. The achieved bit rates are 80 Gbit/s, which are about two orders of magnitude larger than for currently commercially available all-electronic TRNGs. Further developments of the proposed TRNG methods may lead to a miniaturized, on-chip, high-speed TRNG with verified randomness.

The synchronization of spontaneous chaotic current self-oscillations of weakly coupled GaAs/Al_{0.45}Ga_{0.55}As SL devices has been demonstrated as a useful building block for various tasks in secure communications. The emergence of several types of chaos synchronization, e.g. leader-laggard, face-to-face, and zero-lag synchronization in network patterns of coupled SLs consisting of unidirectional and mutual coupling as well as self-feedback coupling has been experimentally demonstrated. Each type of synchronization clearly reflects the symmetry of the topology of its network pattern. The emergence of a chaotic SL oscillator without external feedback and synchronization among differently structured SLs open up the possibility for advanced secure multi-user communication methods based on large networks of coupled SLs.

Acknowledgements The authors would like to thank Y. Y. Huang, W. Li, H. Qin, H. Song, as well as Z. Z. Yin from the Key Laboratory of Nanodevices and Applications, Suzhou Institute of Nano-Tech and Nano-Bionics, Chinese Academy of Sciences, Suzhou, China, I. Kanter, I. Reidler, as well as M. Rosenbluh from the Department of Physics, Bar-Ilan University, Ramat-Gan, Israel, K. Biermann from the Paul-Drude-Institut für Festkörperelektronik, Leibniz-Institut im Forschungsverbund Berlin e. V., Berlin, Germany, and Luis L. Bonilla, M. Carretero, as well as M. Ruiz-García from the Gregorio Millán Institute for Fluid Dynamics, Nanoscience and Industrial Mathematics, Universidad Carlos III de Madrid, 28911 Leganés, Spain, for their continuous and fruitful contributions as well as L. Schrottke from the Paul-Drude-Institut für Festkörperelektronik, Leibniz-Institut im Forschungsverbund Berlin e. V., Berlin, Germany, and Stephen Teitworth from the Department of Physics, Duke University, Durham, North Carolina, USA, for a critical reading of the manuscript.

References

1. Y.H. Zhang, J. Kastrup, R. Klann, K.H. Ploog, H.T. Grahn, Phys. Rev. Lett. **77**, 3001–3004 (1996)
2. Y.Y. Huang, W. Li, W.Q. Ma, H. Qin, Y.H. Zhang, Chin. Sci. Bull. **57**, 2070–2072 (2012)

3. W. Li, I. Reidler, Y. Aviad, Y.Y. Huang, H. Song, Y.H. Zhang, M. Rosenbluh, I. Kanter, *Phys. Rev. Lett.* **111**, 044102, 5 (2013)
4. https://en.wikipedia.org/wiki/Comparison_of_hardware_random_number_generators
5. W. Li, Y. Aviad, I. Reidler, H. Song, Y.Y. Huang, K. Biermann, M. Rosenbluh, Y.H. Zhang, H.T. Grahn, I. Kanter, *Europhys. Lett.* **112**, 30007, 5 (2015)
6. L.L. Bonilla, H.T. Grahn, *Rep. Prog. Phys.* **68**, 577–683 (2005)
7. Y.H. Zhang, R. Klann, H.T. Grahn, K.H. Ploog, *Superlattices Microstruct.* **21**, 565–568 (1997)
8. L.L. Bonilla, M. Alvaro, M. Carretero, *J. Math. Ind.* **7**(1), 1–17 (2017)
9. Y.Y. Huang, W. Li, W.Q. Ma, H. Qin, H.T. Grahn, Y.H. Zhang, *Appl. Phys. Lett.* **102**, 242107, 3 (2013)
10. Z.Z. Yin, H. Song, Y.H. Zhang, M. Ruiz-García, M. Carretero, L.L. Bonilla, K. Biermann, H.T. Grahn, *Phys. Rev. E* **95**, 012218, 7 (2017)
11. M. Alvaro, M. Carretero, L.L. Bonilla, *Europhys. Lett.* **107**, 37002, 6 (2014)
12. Y.Y. Huang, H. Qin, W. Li, S.L. Lu, J.R. Dong, H.T. Grahn, Y.H. Zhang, *Europhys. Lett.* **105**, 47005, 5 (2014)
13. I. Kanter, Y. Aviad, I. Reidler, E. Cohen, M. Rosenbluh, *Nat. Photon.* **4**, 58–61 (2009)
14. NIST Statistical Test Suite at http://csrc.nist.gov/groups/ST/toolkit/rng/stats_tests.html